The Effects of CaF_2, Basicity, and Atmospheric Conditions on the Solubility of Carbon and Nitrogen in the CaO-SiO_2-Al_2O_3-Based Slag System

JUN-YONG PARK and IL SOHN

The solubility of carbon and nitrogen in the CaF_2-CaO-SiO_2-Al_2O_3 slag system was studied. The effects of the CaF_2, extended basicity ($CaO/(SiO_2 + Al_2O_3)$), and atmospheric conditions on the dissolution behavior of the carbon and nitrogen, as well as the correlations of the behaviors with the slag structure observed at 1773 K (1500 °C), are presented. Increases in the extended basicity and the CaF_2 increased the solubility of carbon in the slag. In the case of nitrogen dissolution, a characteristic parabolic curve with an identifiable minimum was observed for the slag. This curve shape correlated with a change in the dominant mechanism of dissolution from an incorporated to a free nitride. The solubility of carbon in the mixture of CO with N_2 was significantly higher than that of carbon in the mixture of CO with Ar and is likely due to the formation of cyanide. Thus, when carbon is present in significant quantities in the slag, the solubility of nitrogen in the slag increases. The degree of depolymerization of the slag with increased content of $CaO/(SiO_2 + Al_2O_3)$ and CaF_2 was verified using Fourier transform infrared and Raman spectroscopy.

DOI: 10.1007/s11663-012-9765-9

I. INTRODUCTION

ADVANCED high-strength steels, such as transformation-induced plasticity (TRIP) and twinning-induced plasticity (TWIP), often have high concentrations of aluminum in common. During casting, the Al in these steel grades reacts with the SiO_2 in the mold flux to increase the alumina (Al_2O_3) content of the slag. The oxide constituents of slag can be classified as basic or acidic depending on the tendency of the oxide either to donate or to accept/consume free oxygen ions,[1] respectively. Al_2O_3, on the other hand, is classified as an amphoteric oxide, and can behave either as a basic or an acidic component. Changes in the Al_2O_3 concentrations in the flux can alter the dissolution capacity of the slag, including both its nitrogen and carbon dissolution capacities. As the capacity of the slag changes, the redistribution of interstitial elements, such as the carbon and nitrogen, between the slag and the metal can contribute to chemical deviations in the resulting semi-finished product that is formed during the continuous casting process; this phenomenon has been previously observed during actual casting processes.

Due to the dynamic, relative changes in the Al_2O_3 concentration of the melted flux during the casting of TRIP and TWIP steels, the additions of the CaF_2-containing cuspidine phase may also be reduced, which has direct implications for the designing of steel mold fluxes that contain high quantities of Al. Thus, the variations in the content of CaF_2 may also affect the nitride and carbide dissolution capacities of the flux. Carbon dissolves in ionic melts according to Reaction [1], and the carbide capacity can be defined by Eq. [2][2–5]:

$$2C(s) + O^{2-} = C_2^{2-} + 1/2O_2(g) \quad [1]$$

$$C_{C_2^{2-}} = \frac{K_1 \times a_{O^{2-}}}{f_{C_2^{2-}}} = \frac{(\text{mass pct } C_2^{2-}) \times P_{O_2}^{1/2}}{f_{C_2^{2-}}} \quad [2]$$

where K_1, a_i, $f_{C_2^{2-}}$, and P_{O_2} are the equilibrium constant, activity of species i, activity coefficient of C_2^{2-} ions, and oxygen partial pressure of Reaction [1], respectively. Kuwata and Suito[2] demonstrated that the carbon distribution ratios were dependent on the oxygen potential with a slope of 1/2 in the CaO-Al_2O_3 binary system. Park *et al.*[4] suggested that in the CaO-Al_2O_3-CaF_2 slag system, the carbide capacity could be increased by higher ratios of CaO/Al_2O_3 at a fixed CaF_2 content and with an increased CaF_2 content (up to 25 mol. pct).

Min and Fruehan,[6] Sohn *et al.*,[7] and Martinez and Sano[8] reported that nitrogen dissolves in molten slag as either a free nitride (N^{3-}) or as an incorporated nitride (N^-), depending on the slag composition. In an acidic slag of low basicity, the nitrogen reacted with the non-bridged oxygen (O^-) as an incorporated nitride, shown in Reaction [3]. However, in a basic slag system, the nitrogen reacted with the free oxygen (O^{2-}) as a free nitride, shown in Reaction [4], given below:

JUN-YONG PARK, Graduate Student, and IL SOHN, Associate Professor, are with the Yonsei University, 262 Seongsanno, Seodaemun-Gu, Seoul 120-749, South Korea. Contact e-mail: ilsohn@yonsei.ac.kr

Manuscript submitted June 13, 2012.
Article published online November 30, 2012.

$$\text{Incorporated nitride: } 1/2\ N_2(g) + 2O^- = N^- + 1/2O^{2-} + 3/4O_2(g) \quad [3]$$

$$\text{Free nitride: } 1/2\ N_2(g) + 3/2O^{2-} = N^{3-} + 3/4O_2(g) \quad [4]$$

The corresponding dissolution capacities of the slag can be obtained with Eqs. [5] and [6], which are given as follows[9]:

$$\text{Incorporated nitride: } C_{N^-} = \frac{(\text{mass pct } N^-) \times P_{O_2}^{3/4}}{P_{N_2}^{1/2}} = \frac{K_3 \cdot a_{O^-}^2}{a_{O^{2-}}^{1/2} \cdot f_{N^-}} \quad [5]$$

$$\text{Free nitride: } C_{N^{3-}} = \frac{(\text{mass pct } N^{3-}) \times P_{O_2}^{3/4}}{P_{N_2}^{1/2}} = \frac{K_4 \cdot a_{O^{2-}}^{3/2}}{f_{N^{3-}}} \quad [6]$$

where $K_{(i)}$, a_i, f_i, and P_{O_2} are the equilibrium constant of the reaction (i), activity of species i, activity coefficient of species i, and oxygen partial pressure, respectively. When both carbon and nitrogen coexist, there is a tendency for cyanide to form in the slag, which can increase the total nitrogen and carbon solubility *vs* the solubility tendency based on the individual reactions alone. According to the past literature,[1,10–12] the formation of cyanide and its capacity can be represented by Eqs. [7] and [8] as follows:

$$1/2O^{2-} + C(s) + 1/2N_2(g) = CN^- + 1/4O_2(g) \quad [7]$$

$$C_{CN^-} = \frac{(\text{mass pct } CN^-) \times P_{O_2}^{1/4}}{P_{N_2}^{1/2}} = \frac{K_7 \cdot a_{O^{2-}}^{1/2}}{f_{CN^-}} \quad [8]$$

where $K_{(i)}$, a_i, f_i, and P_{O_2} are the equilibrium constant of reaction (i), activity of species i, activity coefficient of species i, and oxygen partial pressure, respectively.

In this study, the solubility of carbon and nitrogen at 1773 K (1500 °C) in the $CaO\text{-}SiO_2\text{-}Al_2O_3\text{-}CaF_2$ slag system, which comprises the bulk of the composition of TRIP and TWIP mold fluxes, was investigated. The effects of the apparent extended basicity ($CaO/(Al_2O_3 + SiO_2)$), the content of CaF_2, and various atmospheric conditions (*e.g.*, CO with Ar gas and CO with N_2 gas) on the solubility of carbon and nitrogen were observed. The solubility was correlated with the slag structure using Fourier transform infrared (FTIR) spectroscopy and Raman analysis of the fluxes, which were quenched at 1773 K (1500 °C).

II. EXPERIMENTAL PROCEDURE

A. *Experimental Method and Analysis of the Carbon and Nitrogen Content*

Samples were synthesized using the following reagent-grade chemicals (Junsei; Tokyo, Japan): $CaCO_3$ (99.5 pct), SiO_2 (99.5 pct), Al_2O_3 (99 pct), and CaF_2 (99 pct). A total of 4 g of each slag sample was premelted in an inert Pt-10 wt pct Rh crucible (OD: 1.4 cm, ID: 1.2 cm, H: 4.1 cm) for 5 hours at 1773 K (1500 °C) under 250 sccm of Ar gas until samples of homogeneous composition were obtained. The post-experimental chemical compositions are listed in Table I and were determined by X-ray fluorescence spectroscopy (XRF; S4 Explorer; Bruker AXS GmbH, Karlsruhe, Germany). A schematic of the experimental setup is shown in Figure 1. Each 4-g slag sample was maintained in a carbon crucible (OD: 1.5 cm, ID: 1.1 cm, H: 7.2 cm) under a mixture of CO with Ar or N_2 gases (6:4) at 250 sccm and was then injected into the reaction tube of a $Mo\text{-}Si_2$ (Kanthal; Hallstahammer, Sweden) vertical resistance furnace at 1773 K (1500 °C). The oxygen partial pressure of the gas mixture can be calculated

Table I. Experimental Composition and Carbon, Nitrogen Solubility of the $CaO\text{-}SiO_2\text{-}Al_2O_3\text{-}CaF_2$ Slag System in the Present Study at 1773 K (1500 °C)

	Composition (Wt Pct)				Carbon (Wt Pct)		Nitrogen (Wt Pct)		
Sample No.	CaO	SiO_2	Al_2O_3	CaF_2	AVG	STDEV	AVG	STDEV	Basicity C/(S + A)
FCSF1	40.170	9.470	10.000	10.360	0.081	0.001	…	…	0.81
FCSF2	45.160	9.610	35.000	10.230	0.096	0.001	…	…	1.01
FCSF3	50.090	9.500	30.900	9.510	0.096	0.001	…	…	1.24
FCSF4	50.880	9.120	40.000	0.000	0.070	0.002	…	…	1.04
FCSF5	48.000	9.310	37.500	5.190	0.063	0.001	…	…	1.03
FCSF6	43.860	9.340	32.500	14.290	0.121	0.002	…	…	1.05
FCSFln	42.100	8.100	40.000	9.800	0.212	0.013	1.748	0.100	0.88
FCSF2n	47.390	8.610	35.000	9.000	0.397	0.001	0.995	0.126	1.09
FCSF2′n	47.840	8.170	35.000	9.000	0.409	0.003	1.140	0.368	1.11
FCSF3n	48.210	9.990	30.900	10.900	0.648	0.009	3.211	0.399	1.18
FCSF4n	51.710	8.290	40.000	0.000	0.254	0.003	1.530	0.063	1.07
FCSF5n	50.600	8.400	37.500	3.490	0.327	0.010	0.606	0.098	1.10
FCSF6n	44.110	8.580	32.500	14.810	0.498	0.003	1.361	0.003	1.07

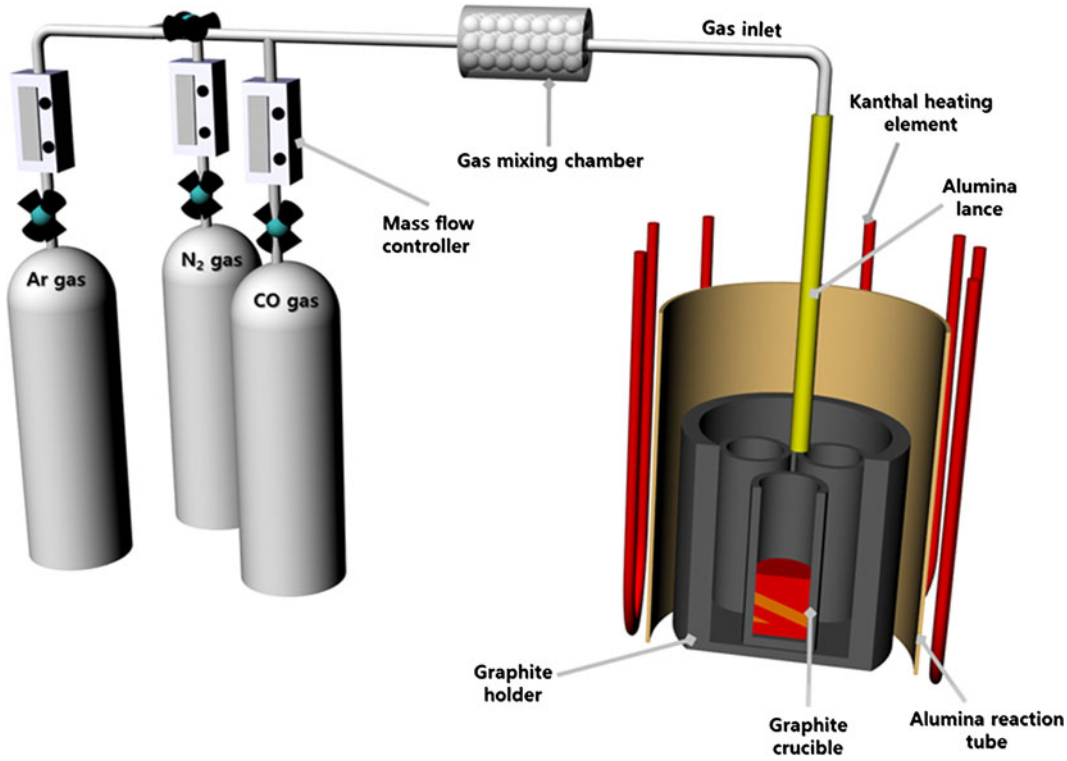

Fig. 1—Schematic of the experimental apparatus.

from Eq. [9] using the C/CO equilibrium reaction as follows[13]:

$$\mathrm{C(s)} + \frac{1}{2}\mathrm{O_2(g)} = \mathrm{CO(g)}$$
$$\Delta G^\circ = -114,000 - 85.8T\ (\mathrm{J/mol}) \qquad [9]$$

The experimental temperature was calibrated with a B-type reference thermocouple, and the furnace temperature was controlled to within ±3 K using a proportional-integral-derivative (PID) controller. Preliminary experiments were conducted to determine the equilibrium reaction time of the slag/carbon; the results of these experiments are presented in Figure 2. It was found that equilibrium could be reached within 18 hours; thus, the equilibration time was generally assumed to be 24 hours. After a sufficient degree of reaction had been obtained, the slag sample was quickly removed from the furnace and quenched with Ar gas. The cooling rate of Ar gas quenching is not precisely known, yet the absence of any characteristic peaks in the X-ray diffraction (XRD; Ultima IV; Rigaku, Tokyo, Japan) pattern shown in Figure 3 indicates that Ar quenching imparts a sufficient cooling rate to obtain a glassy structure. All samples were stored in a desiccator and were then analyzed for their carbon and nitrogen content within 24 hours. The carbon and nitrogen content was measured by a CS-300 and a TC-300 N/O analyzer (LECO; St. Joseph, MI, USA).

B. *Analysis of the Slag Structure Using FTIR Spectroscopy*

The structures of the as-quenched slag samples were analyzed with FTIR (Spectrum-100; PerkinElmer, Waltham, MA, USA) and Raman (PD-RSM300; Photon Design, Tokyo, Japan) spectroscopic methods. A total of 2 mg of the sample was mixed with 200 mg of KBr, and the mixture was then pressed into pellets with a diameter of 10 mm and a thickness of 1 mm. The FTIR and Raman transmission spectra were restricted from 1400 to 400 $\mathrm{cm^{-1}}$. This range was used to select the various symmetric stretching, asymmetric stretching, and bending vibrational modes of the Si-O and Al-O bonds, which comprise the majority of the slag network structure. Figure 4 presents typical FTIR spectra of the as-quenched slag samples. The symmetric stretching bands of the tetrahedral Si-O bonds can be observed in the range from 1100 to 850 $\mathrm{cm^{-1}}$,[14–17] where the bonds are a spectral convolution of the NBO/Si = 1-, 2-, 3-, and 4-unit silicate structure. The NBO/Si numeral is a measure of the number of non-bridged oxygen atoms per Si atom that are contained in the silicate anion structure. The identification of a lower NBO/Si number at a higher wavenumber suggests the presence of a more complex and highly polymerized structure. The asymmetric $[\mathrm{AlO}_n\mathrm{F}_{4-n}]$-tetrahedral stretching band is located near 940 to 720 $\mathrm{cm^{-1}}$,[18,19] and the symmetric stretching of the $[\mathrm{AlO_4}]$-tetrahedral band is primarily located within the 700 to 600 $\mathrm{cm^{-1}}$ range.[20–23] The bands from 600 to 400 and 450 $\mathrm{cm^{-1}}$ correspond to the asymmetric

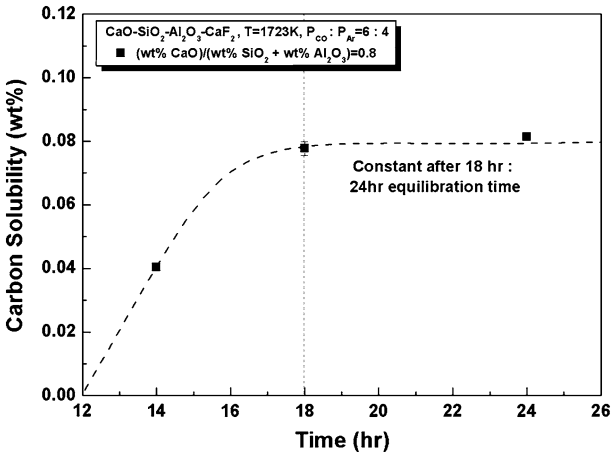

Fig. 2—Preliminary experiments to determine the equilibration times in the $CaO-SiO_2-Al_2O_3-CaF_2$ slags at 1773 K (1500 °C).

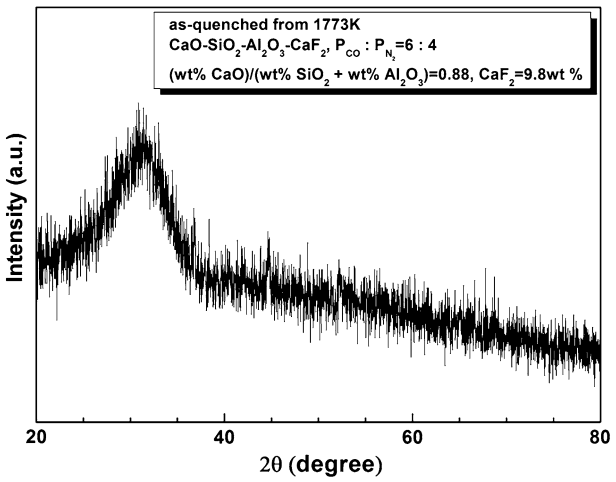

Fig. 3—A typical XRD pattern of an as-quenched slag sample from 1773 K (1500 °C).

stretching vibrations of the $[AlO_6]$-octahedral[21,24,25] and the deformational vibration of either the Si-O-Si or the Si-O-Al bonds, respectively.[26] These results are summarized in Table II.

C. *Analysis of the Slag Structure Using Raman Spectroscopy*

Raman spectroscopy (PD-RSM300; Photon Design; Tokyo, Japan), with a 514-nm laser, was used for further analysis of the slag structures. Similar to the FTIR spectra, the analysis of the Raman spectra was constrained from 1200 to 400 cm^{-1}, and the area fractions and quantitative amounts of the individual silicate and aluminate bonds were ascertained by deconvoluting the Raman spectra with Peak Fit V4 software (Systat Software Inc.; Chicago, WA, USA). The deconvolution was performed using a non-parametric baseline. Figure 5 displays a typical resulting deconvolution of a Raman spectrum; this particular deconvolution was obtained from a sample with 9.8 wt pct CaF_2 content at a fixed apparent extended basicity of 0.88, which is defined as $CaO/(SiO_2 + Al_2O_3)$, and under a CO and N_2 atmosphere with a ratio of 6:4. The Raman bands with peaks at approximately 1092, 948, 881, and 831 cm^{-1} have been identified to be the symmetric stretching vibrations corresponding to NBO/Si of 1, 2, 3, and 4, respectively.[26,27] The bands at 1151 and 1005 cm^{-1} can be assigned to the asymmetric silicon-oxygen stretching motions of the fully polymerized silica-glass framework with an NBO/Si ratio equal to 0.[28,29] The band at approximately 768 cm^{-1} was determined to be the $[AlO_nF_{4-n}]$ stretching vibration,[18,19] which occurs in a similar region to that observed in the FTIR analysis. The bands with peaks at approximately 607, 548, and 463 cm^{-1} were identified as corresponding to the symmetric stretching vibration of $[AlO_4]$-tetrahedra,[20–23] the asymmetric stretching vibration of $[AlO_6]$-octahedra,[15,27,30] and the Si-O-Si(Al) vibrations,[31,32] respectively.

III. RESULTS AND DISCUSSION

A. *Effect of CaF_2 on the Solubility of Carbon in the $CaO-SiO_2-Al_2O_3$ Slag System at a Fixed Extended Basicity*

Figure 6 presents the solubility of carbon as a function of the CaF_2 content (0, 5, 10 and 15 wt pct) and with a fixed extended basicity of approximately 1.0 to 1.1. The carbon solubility increases linearly with increased CaF_2 content. According to Reaction [1], the addition of CaF_2 to slag supplies additional fluorine ions, which act as a network modifier; that is, the fluorine ions free the bridged oxygen ions by displacing them from the slag structure. The increase in free oxygen ions increases the basicity of the slag, which pushes Reaction [1] to the product side and increases the formation of carbide in the slag. A comparison of the present study with Park *et al.*[4] showed a similar trend, but the different oxygen and nitrogen partial pressures of the present study resulted in different absolute values of the carbon content in the slag.

B. *The Effect of Basicity on the Solubility of Carbon in the $CaO-SiO_2-Al_2O_3$ Slag System with a Fixed CaF_2 Content*

Figure 7 shows the solubility of carbon in the $CaO-SiO_2-Al_2O_3-CaF_2$ slag system as a function of the extended basicity ($CaO/(SiO_2 + Al_2O_3)$) at a fixed CaF_2 content (approximately 9 to 10 wt pct). The carbon solubility increases continuously with increased basicity regardless of the gas atmosphere; however, for gas mixtures of CO with N_2, the carbon solubility increases significantly with increasing basicity of the slag system. At a higher extended basicity, excess O^{2-} is available, which increases the oxygen ion activity ($a_{O^{2-}}$), pushes reaction [4] to the product side, and subsequently increases the C_2^{2-} content of the slag.

The significant increase in the solubility of carbon in the presence of the CO and N_2 mixture is presumed to be due to the formation of CN^-, as described by Eq. [7]. In the presence of nitrogen and as the slag basicity

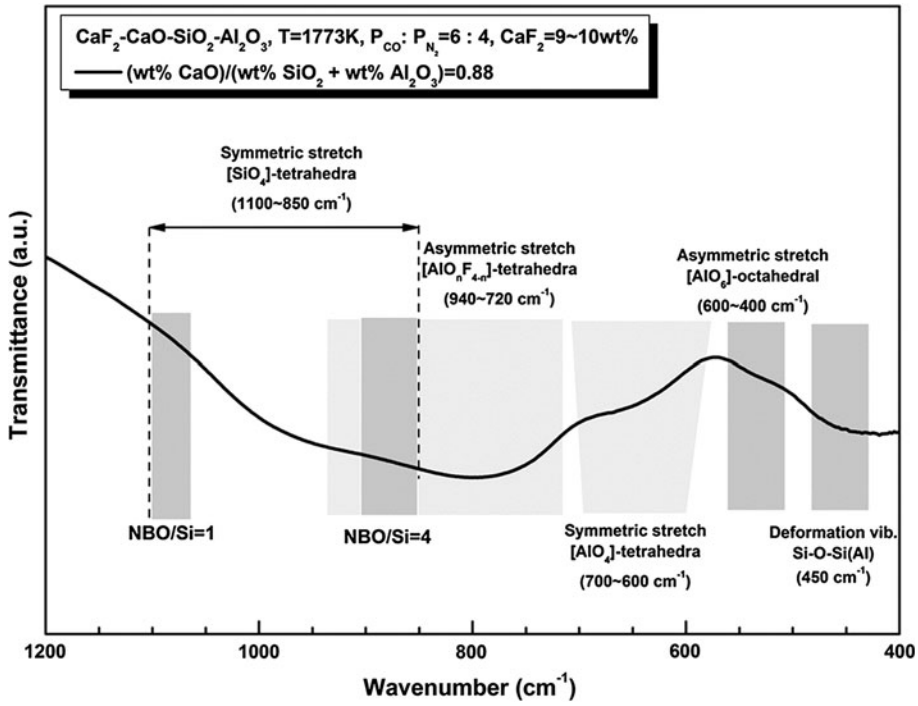

Fig. 4—Typical FTIR spectra for the $CaO-SiO_2-Al_2O_3-CaF_2$ slag sample with 4.5 wt pct CaF_2 at extended basicity of 0.88 as quenched from 1773 K (1500 °C).

Table II. FTIR and Raman Data from Published Literature

Mode	Species	Wave Number (cm^{-1})	Refs.
Silicate structure			
Symmetric stretching vibrations	NBO/Si = 1	1100	
	NBO/Si = 2	950 to 980	[14–17, 26, 27]
	NBO/Si = 3	900 to 920	
	NBO/Si = 4	850 to 880	
Asymmetric stretching vibrations	NBO/Si = 0	1060	[28, 29]
		1190	
Aluminate structure			
Symmetric stretching vibrations	$[AlO_4]$-tetrahedral	600 to 700	[20] through [23]
Asymmetric stretching vibrations	$[AlO_6]$-octahedral	400 to 600	[15, 21, 24, 25, 27, 30]
	$[AlO_nF_{4-n}]$-tetrahedral	720 to 940	[18, 19]
Combined structure			
Deformation vibration	Si-O-Si(Al)	~450	[26, 31, 32]

increases, the formation of CN^- is accelerated, and the solubility of carbon in the slag tends to increase. This speculation was partially verified by preliminary experiments done on several slag samples where carbon and nitrogen were both present. Using the ASTM D7237-10 flow injection analysis using gas diffusion separation and amperometric detection, a CN^- of approximately 0.08 to 0.12 wt pct was found. The results clearly indicated significant amounts of CN^- in the melt when nitrogen is present in the slag, but quantitative and accurate results required more than 300 g of slag, and a separate analysis in the present study was impractical. A more quantitative cyanide analysis will be provided in subsequent literature by the present authors.

C. *The Effect of CaF_2 on the Solubility of Nitrogen in the $CaO-SiO_2-Al_2O_3$ Slag System at a Fixed Extended Basicity*

Figure 8 shows the solubility of nitrogen as a function of the CaF_2 content while under a CO and N_2 mixture (at a ratio of 6:4) and at a fixed extended basicity of approximately 1.0 to 1.1. The dissolution behavior of nitrogen as a function of CaF_2 exhibits a parabolic shape similar to that given in Figure 8. At the present slag composition, with an extended basicity from 1.0 to 1.1, the solubility of nitrogen decreases with initial additions of CaF_2 (up to 4 wt pct) until a minimum solubility is reached; at this point, the solubility of nitrogen then increases with additions of CaF_2 (in excess of 4 wt pct).

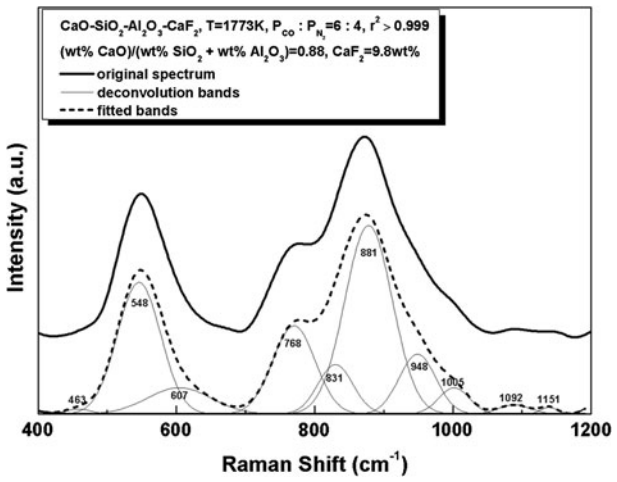

Fig. 5—Typical deconvoluted Raman spectra of the CaO-SiO_2-Al_2O_3-CaF_2 slag sample with 9.8 wt pct CaF_2 at a basicity (C/S + A) of 0.88 as quenched from 1773 K (1500 °C).

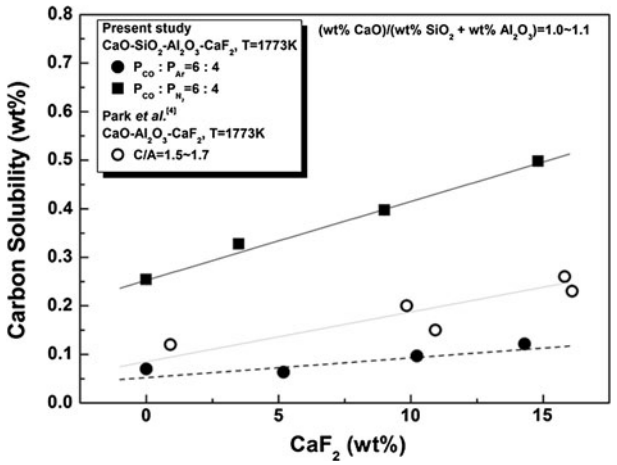

Fig. 6—Carbon solubility as a function of the CaF_2 contents at fixed basicity of 1.0 to 1.1 under different gas atmospheres at 1773 K (1500 °C).

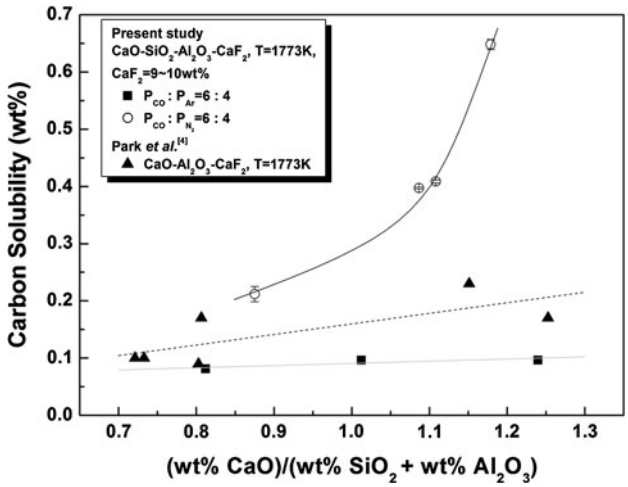

Fig. 7—Carbon solubility as a function of the basicity at fixed CaF_2 contents of 9 to 10 wt pct under different atmosphere at 1773 K (1500 °C).

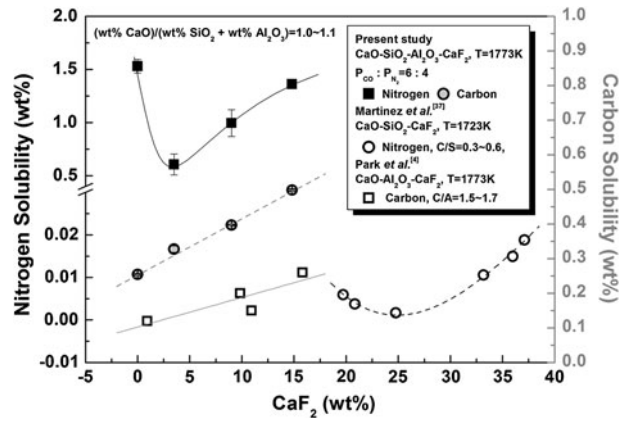

Fig. 8—Carbon and nitrogen solubility as a function of the CaF_2 contents at fixed basicity of 1.0 to 1.1 under CO with N_2 mixed atmosphere at 1773 K (1500 °C).

This is comparable to the effect of extended basicity, in which the nitrogen dissolution behavior changes from an incorporated nitride mechanism to a free nitride mechanism. With additions of CaF_2 of up to 4 wt pct in the slag, the slag system with an extended basicity of 1.0 to 1.1 is at an intermediate basicity, at which the dominant dissolution behavior is likely to arise from the incorporated nitride; thus, the CaF_2 additions decrease the activity of the non-bridged oxygen in Reaction [4]. This is accomplished by the breaking of non-bridged oxygen bonds by F^-; this process then releases the free oxygen ions, resulting in decreased nitrogen solubility. However, above 4 wt pct CaF_2, the slag system becomes basic with the availability of excess O^{2-}, and the nitrogen dissolution behavior no longer follows the incorporated nitride mechanism, but rather the free nitride mechanism. At this CaF_2 content, further additions of CaF_2 substitute with the non-bridged oxygen, releasing O^{2-} into the slag and subsequently increasing the activity of the free oxygen (a_{O_2-}), which in turn increases the nitrogen solubility. The results of several past publications are also included in Figure 8.

D. *The Effect of the CaF_2 Content and the Basicity on the Slag Structure Using FTIR and Raman Spectroscopy*

Figure 9 shows the FTIR spectra as a function of the wavenumber (cm^{-1}) with various CaF_2 contents and a fixed basicity of 1.10. The FTIR spectra were focused within the wavenumber range of 1200 to 400 cm^{-1}, in which the dominant silicate and aluminate structures exist. The FTIR spectra contain convoluted vibrations of stretching and bending of the various structural species within the melt. From the 1100 to 850 cm^{-1} range, the symmetric stretching vibrations of NBO = 1 to NBO/Si = 4 are observed and one of the asymmetric stretching vibrations of the highly complex NBO/Si = 0 is observed. A pronounced trough of the NBO/Si = 0 suggests a highly complex and polymerized structure of the melt. To qualitatively compare the amount of the

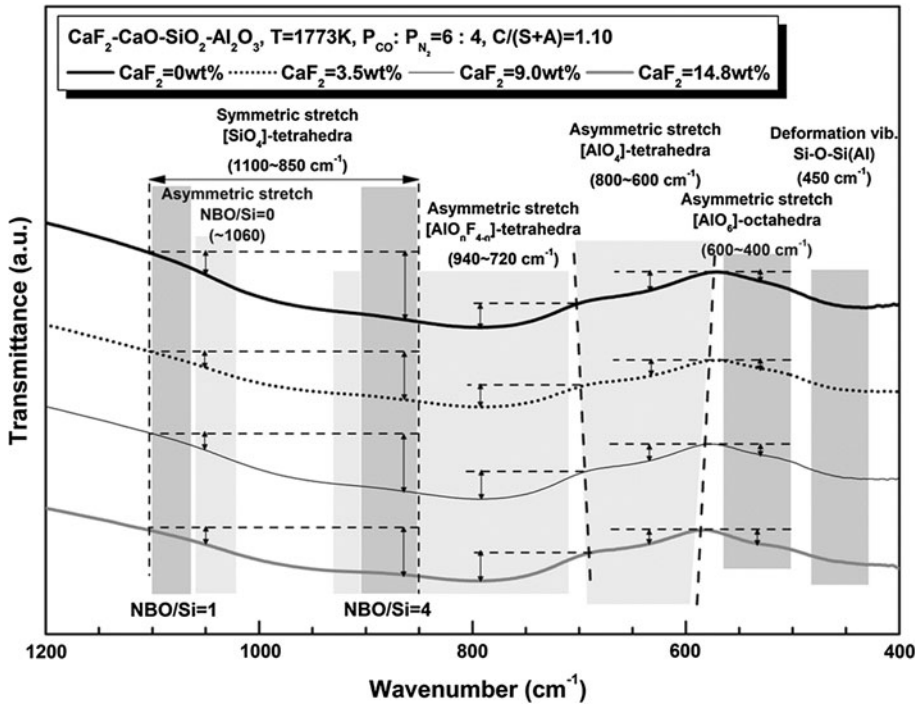

Fig. 9—The FTIR transmittance spectra as a function of wavenumber (cm^{-1}) at various CaF_2 contents and at fixed basicity of 1.1 under CO and N_2 mixed atmosphere as quenched from 1773 K (1500 °C).

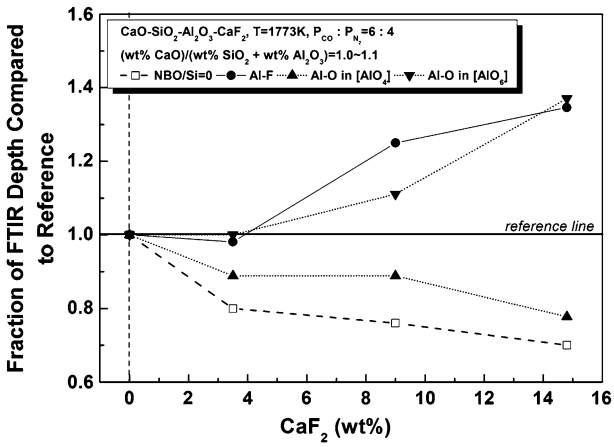

Fig. 10—The variation in the fraction of the FTIR transmittance depth as a function of CaF_2 contents with respect to the reference sample of CaF_2-free slag for a fixed basicity of 1.0 to 1.1 under CO and N_2 mixed atmosphere as quenched from 1773 K (1500 °C).

NBO/Si = 0 from the FTIR convoluted spectra for the various slag compositions, a horizontal baseline shown by the dashed line which intersects with the FTIR spectra at 1100 cm^{-1} was chosen. The subsequent depth of the trough is measured and the CaF_2-free sample is taken as the reference to calculate the fraction. For the Al-F and Al-O in the tetrahedral and octahedral configuration, the baseline for measuring the trough depth is chosen at the peaks of the characteristic FTIR transmittance range for the various Al-F and Al-O structural species. Figure 10 presents the change in peak depth of the FTIR spectra shown in Figure 9 for the various bonds of Si-O and Al-O relative to the reference FTIR spectra with 0 wt pct CaF_2. In Figure 10, both the highly complex structure of NBO/Si, which is equal to 0, and the $[AlO_4]$-tetrahedral band decrease with increasing CaF_2 content; however, the relative size of the $[AlO_6]$-octahedral and $[AlO_nF_{4-n}]$-tetrahedral bands increases with increasing CaF_2 content. In Figure 10, the highly complex bands of the NBO/Si = 0 and $[AlO_4]$-tetrahedral structures tend to decrease, while the $[AlO_6]$-octahedral and $[AlO_nF_{4-n}]$-tetrahedral bands increase with higher CaF_2. With increasing CaF_2 content, the silicate and aluminate structures are depolymerized, which is the typical consequence of using a basic oxide and network modifier. As the CaF_2 content is increased, the slag structure depolymerizes and the content of excess free oxygen ions increases, which affects the solubility of carbide and nitrogen in a similar manner to the effect of increasing $CaO/(SiO_2 + Al_2O_3)$. It should be noted that Hayashi *et al.*,[33] using MAS-NMR (magic angle spin-nuclear magnetic resonance), showed fluorine ions to be coordinated near the Ca^{2+} cations, and thus CaF_2 additions to the slag and subsequent structural modifications in the slag do not occur. However, the present work using FTIR and Raman clearly seems to indicate significant modifications in the vibrations of the Al-O and Al-F in the various complex structural units with CaF_2 additions into the slag resulting also in modified carbon and nitrogen contents.

Figure 11 shows the effect of basicity on the FTIR transmittance trough as a function of the wave number (cm^{-1}) at a fixed CaF_2 content (approximately 9 to

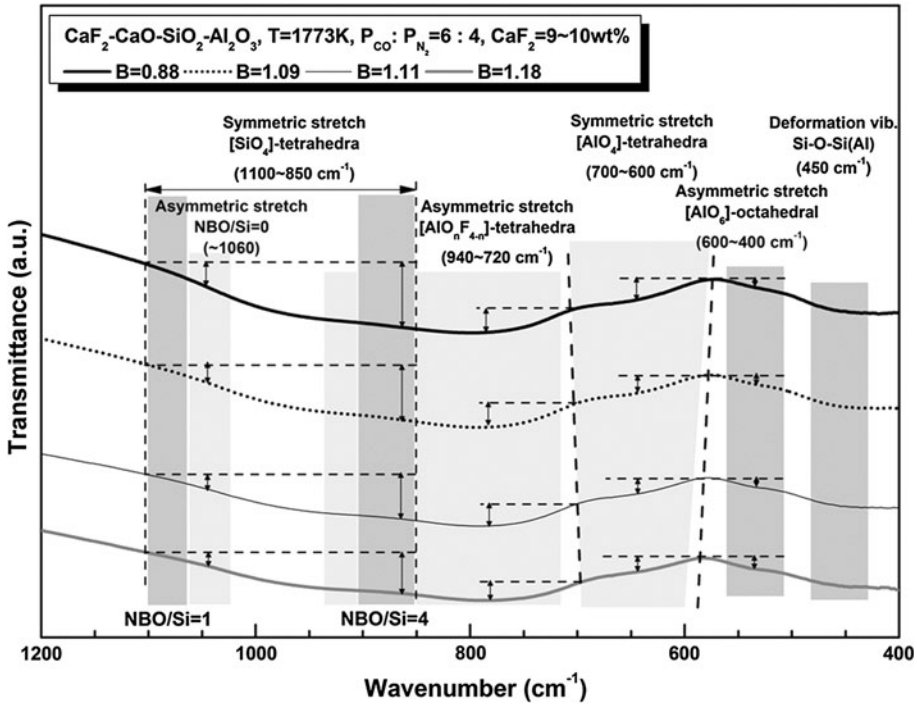

Fig. 11—The FTIR transmittance trough as a function of wavenumber (cm^{-1}) for fixed CaF_2 contents of 9 to 10 wt pct and varying basicity of 1.0 to 1.1 under CO and N_2 mixed atmosphere as quenched from 1773 K (1500 °C).

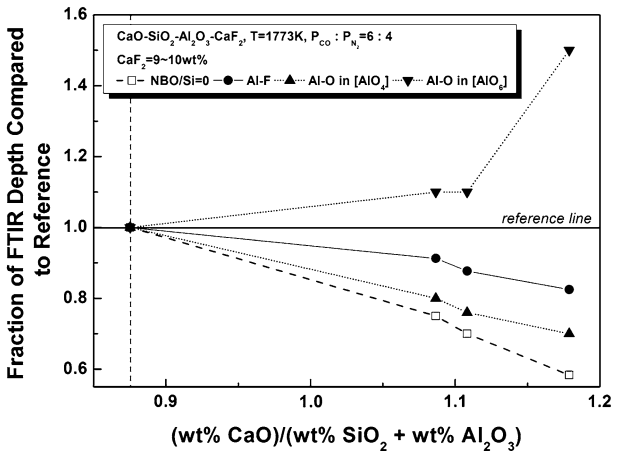

Fig. 12—The variation in the fraction of the FTIR transmittance depth as a function of basicity for fixed CaF_2 contents with respect to the reference sample of 0.88 basicity slag of 9 to 10 wt pct and varying basicity under CO and N_2 mixed atmosphere as quenched from 1773 K (1500 °C).

10 wt pct). Figure 12 is comparable to Figure 10, but the reference of the FTIR peak bands is the slag with an extended basicity of 0.88. Considering that the highly polymerized NBO/Si = 0 and $[AlO_4]$-tetrahedral structures decrease with increasing basicity, it can be inferred that the silicate and aluminate structures have a tendency to become depolymerized with increasing basicity. Therefore, the slag structure depolymerizes and releases oxygen ions until the oxygen ion content is in excess; during the depolymerization process, the complex network structure is simplified to dimers or monomers.

As depolymerization continues, an increasing content of the $[AlO_6]$-octahedral configuration suggests an increase in the amount of free oxygen ions available in the slag, which further results in a higher activity of the free oxygen ions. This results is an increased carbide dissolution capacity, according to Reaction [1]. However, the nitride capacity of the slag is dependent on the nitrogen dissolution mechanism of the slag. At low basicity, where bridged oxygen is present, the higher activity of the bridged oxygen (a_{O_0}) increases the incorporated nitride capacity of the slag, but at higher basicity, the higher free oxygen activity ($a_{O_{2-}}$) instead increases the free nitride capacity. Because depolymerization of the slag structure is evident at higher basicity values, the a_{O_0} initially decreases with increasing basicity, which results in the reduced dissolution of nitrogen in the slag. As the slag composition reaches the basic system, the higher basicity results in a higher $a_{O_{2-}}$ and also a subsequent increase in the free nitride content . Due to the qualitative aspect of FTIR analysis, Raman spectroscopy was also employed, which provides a more robust quantitative analysis.

Figure 13 shows the fractions of the various silicate, aluminate, and AlO_nF_{4-n} species after deconvoluting the Raman spectra in the range from 1200 to 400 cm^{-1} and as a function of the CaF_2 content at a fixed basicity (approximately 1.0 to 1.1). After the spectra were subjected to the deconvolution treatments, they were integrated to obtain the area. Based on the integration results, the area fractions of NBO/Si of 1 and 3 both decrease, and the area fraction of NBO/Si of 2 increases with a higher content of CaF_2. This trend suggests that the silicate structures have been depolymerized, as

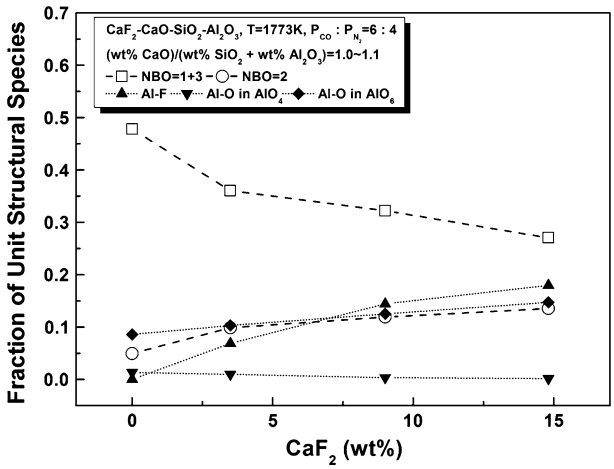

Fig. 13—The fraction of the unit structural species calculated from the deconvoluted Raman spectra as a function of CaF_2 contents for a fixed basicity of 1.0 to 1.1 under CO and N_2 mixed atmosphere.

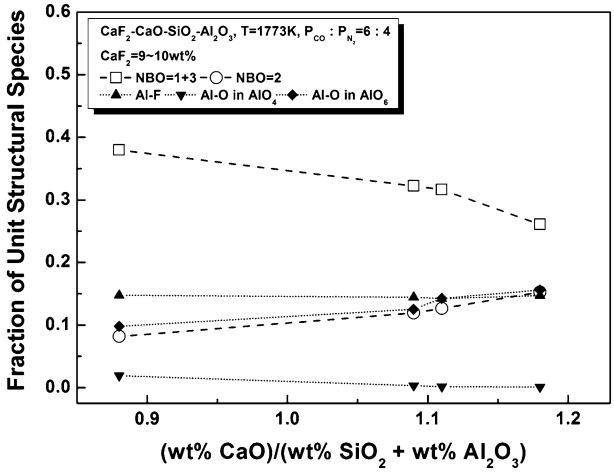

Fig. 14—The fraction of the unit structural species calculated from the deconvoluted Raman spectra as a function of basicity for fixed CaF_2 contents of 9 to 10 wt pct under CO and N_2 mixed atmosphere.

previously suggested by Mysen *et al.*[27] Depolymerization of the aluminate structure is also supported by the observed decrease in the network structure of $[AlO_4]$-tetrahedra and the increase in the network-modified $[AlO_6]$-octahedral bonds at a higher CaF_2 content. The effect of basicity at a fixed content of CaF_2 (approximately 9 to 10 wt pct) is also shown in Figure 14. Similar depolymerization trends can be observed in this figure.

E. *The Effect of Basicity on the Solubility of Nitrogen in the CaO-SiO_2-Al_2O_3 Slag System at a Fixed CaF_2 Content*

Figure 15 shows the solubility of nitrogen in the CaO-SiO_2-Al_2O_3-CaF_2 slag system at a fixed CaF_2 content (approximately 9 to 10 wt pct) as a function of the

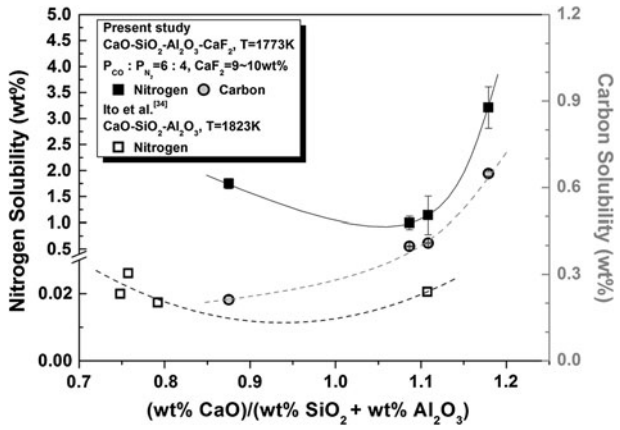

Fig. 15—Carbon and nitrogen solubility as a function of the basicity at fixed CaF_2 contents of 9 to 10 wt pct under CO and N_2 mixed atmosphere at 1773 K (1500 °C).

extended basicity under an atmosphere of CO and N_2 at a ratio of 6:4. The behavior of the nitrogen dissolution mechanism as a function of $CaO/(SiO_2 + Al_2O_3)$ exhibits a characteristic parabolic shape. At low basicity, the solubility of nitrogen decreases with increasing basicity until it reaches a minimum. After the point of minimum solubility, the nitrogen content in the slag instead begins to increase with increasing basicity. The parabolic behavior of the nitrogen dissolution in the slag suggests that two characteristic nitrogen dissolution mechanisms operate in the molten slag depending on the slag basicity, as presented in the aforementioned Reactions [3] and [4]. Reaction [3] represents nitrogen dissolution in slag as an incorporated nitride and Reaction [4] represents nitrogen dissolution as a free nitride. When incorporated nitrides are prevalent in the aluminate structure, the simplest form of the resulting reaction can be expressed by Reaction [10][34]:

$$1/2N_2(g) + 3\left(AlO_3^{3-}\right) = N - 3Al^{2-} + 3/2O^{2-} + 3/4O_2(g) \qquad (10)$$

In the acidic slag system with a low extended basicity, the incorporated nitride dissolution mechanism is inhibited by the increase in activity of the free oxygen ions (O^{2-}), as suggested by Reaction [10]. The observation of a parabolic trend in the dissolution of nitrogen in slag is similar to the findings of Ito and Fruehan.[35] According to Figure 8, the solubility of nitrogen is significantly higher when carbon is present. Thus, if unburnt carbon is retained in the mold flux and significant carbon is present in the slag, the nitrogen content of the metal may redistribute into the flux; in such circumstances, significant metal chemistry deviations can occur.

IV. CONCLUSIONS

The solubility of carbon and nitrogen in the CaO-SiO_2-Al_2O_3-CaF_2 slag system at 1773 K (1500 °C) was

studied to identify the effects of the CaF_2, basicity, and compositions of the gas mixture on both the solubility values and the resulting slag structure. Increases in the extended basicity and the CaF_2 were sufficient to increase the dissolution of carbon in the slag; however, a characteristic parabolic curve, which includes a minimum dissolution value, was observed for the dissolution of nitrogen in the slag. Although both the carbide and cyanide capacities increase with higher free oxygen activity ($a_{O_2^-}$), the $a_{O_2^-}$ produces the opposite effect on the free and incorporated nitrides. Compared with the CO and Ar mixture, the solubility of carbon in the CO and N_2 mixture is significantly higher due to the formation of cyanide. When carbon is present, the solubility of nitrogen in the slag increases significantly. Depolymerization of the slag with higher $CaO/(SiO_2 + Al_2O_3)$ and CaF_2 content was verified using FTIR and Raman spectroscopic methods, which also demonstrated a decrease in the highly complex NBO/Si = 0 and $[AlO_4]$-tetrahedral unit structures.

ACKNOWLEDGMENTS

This study was partially supported by the Brain Korea 21 (BK21) Project at the Division of the Humantronics Information Materials, the National Science Foundation of Korea Project No. 2012-8-0486 and the Priority Research Centers Program through the National Research Foundation of Korea(NRF) funded by the Ministry of Education, Science and Technology(2009-0093823).

REFERENCES

1. N. Sano, W.K. Lu, P.V. Riboud, and M. Maeda: *Advanced Physical Chemistry for Process Metallurgy*, Academic Press, San Diego, CA, 1997.
2. M. Kuwata and H. Suito: *Metall. Mater. Trans. B*, 1996, vol. 28B, pp. 57–64.
3. J.H. Park and D.J. Min: *Metall. Mater. Trans. B*, 1999, vol. 30B, pp. 1045–1052.
4. J.H. Park, D.J. Min, and H.S. Song: *ISIJ Int*., 2002, vol. 42, pp. 127–131.
5. R.A. Berryman and I.D. Sommerville: *Metall. Trans. B*, 1992, vol. 23B, pp. 223–227.
6. D.J. Min and R.J. Fruehan: *Metall. Trans. B*, 1990, vol. 21B, pp. 1025–1032.
7. I. Sohn, D.J. Min, and J.H. Park: *Steel Res*., 1999, vol. 70, pp. 215–220.
8. E.R. Martinez and N. Sano: *Metall. Trans. B*, 1990, vol. 21B, pp. 97–104.
9. F.D. Richardson: *Physical Chemistry of Melts in Metallurgy*, Academic Press, London, U.K., 1974.
10. I.H. Jung: *ISIJ Int*., 2006, vol. 46, pp. 1577–1586.
11. K. Schwerdtfeger and H.G. Schubert: *Metall. Trans. B*, 1977, vol. 8B, pp. 535–540.
12. F. Tsukihashi and R.J. Fruehan: *Metall. Trans. B*, 1986, vol. 17B, pp. 535–540.
13. E.T. Turkdogan: *Physical Chemistry of High Temperature Technology*, Academic Press, New York, NY, 1980.
14. A. Aronne, S. Esposito, and P. Pernice: *Mater. Chem. Phys*., 2011, vol. 51, pp. 163–168.
15. F. Branda, F. Arcobello-Varlese, A. Costantini, and G. Luciani: *J. Non-Cryst. Solids*, 1999, vol. 246, pp. 27–33.
16. L. Stoch and M. Sroda: *J. Mol. Struct*., 1999, vols. 511–512, pp. 77–84.
17. S. Ueda, H. Koyo, T. Ikeda, Y. Kariya, and M. Maeda: *ISIJ Int*., 2000, vol. 40, pp. 739–743.
18. K. Nakamoto: *Infrared and Raman Spectra of Inorganic and Coordination Compounds*, 5th ed., Wiley, New York, NY, 1997.
19. J.H. Park, D.J. Min, and H.S. Song: *ISIJ Int*., 2002, vol. 42, pp. 38–43.
20. S.L. Lin and C.S. Hwang: *J. Non-Cryst. Solids*, 1966, vol. 202, pp. 61–67.
21. G. Leekes, N. Nowack, and F. Schlegelmilch: *Steel Res*., 1988, vol. 59, pp. 406–416.
22. P.F. McMillan, W.T. Petusky, B. Cote, D. Massiot, C. Landron, and J.P. Coutures: *J. Non-Cryst. Solids*, 1996, vol. 195, pp. 261–271.
23. C. Huang and E.C. Behrman: *J. Non-Cryst. Solids*, 1991, vol. 128, pp. 310–321.
24. P. Tarte: *Spectrochim. Acta*, 1967, vol. 23A, pp. 2127–2143.
25. V.Z. Kreitsberga, V.G. Chekhovskii, A.P. Sizonenko, Yu.Ya. Keishs, S.E. Redala, and P.G. Pauksh: *Fizika I khimiya Stekla*, 1991, vol. 17, pp. 953–57.
26. B.O. Mysen, D. Virgo, and F.A. Seifert: *Rev. Geophys. Space Phys*., 1982, vol. 20, pp. 353–383.
27. B.O. Mysen, D. Virgo, and C.M. Scarfe: *Am. Mineral*., 1980, vol. 65, pp. 690–710.
28. G. Lucovsky, C.K. Wong, and W.B. Pollard: *J. Non-Cryst. Solids*, 1983, vols. 59–60, pp. 839–846.
29. G.D. Chukin and V.I. Malevich: *J. Appl. Spectrosc*., 1977, vol. 26, pp. 223–229.
30. B.O. Mysen, D. Virgo, W.J. Harrison, and C.M. Scarfe: *Am. Mineral*., 1980, vol. 65, pp. 900–914.
31. J.T. Kohli, R.A. Condrate, and J.E. Shelby: *Phys. Chem. Glass*., 1993, vol. 34, pp. 81–87.
32. P. McMillan: *Am. Mineral*., 1984, vol. 69, pp. 622–644.
33. M. Hayashi, T. Watanabe, K. Nagata, and S. Hayashi: *ISIJ Int*., 2004, vol. 44, pp. 1527–1533.
34. R.E. Martinez, O.V. Espejo, and F. Manjarrez: *ISIJ Int*., 1993, vol. 33, pp. 48–52.
35. K. Ito and R.J. Fruehan: *Metall. Mater. Trans. B*, 1998, vol. 19B, pp. 419–425.